First isomeric yield ratio measurements by direct ion counting and implications for the angular momentum of the primary fission fragments

V. Rakopoulos,[1,*] M. Lantz,[1,†] A. Solders,[1] A. Al-Adili,[1] A. Mattera,[1] L. Canete,[2] T. Eronen,[2] D. Gorelov,[2] A. Jokinen,[2] A. Kankainen,[2] V. S. Kolhinen,[2,‡] I. D. Moore,[2] D. A. Nesterenko,[2] H. Penttilä,[2] I. Pohjalainen,[2] S. Rinta-Antila,[2] V. Simutkin,[1,§] M. Vilén,[2] A. Voss,[2] and S. Pomp[1]

[1]*Department of Physics and Astronomy, Uppsala University, Uppsala 75120, Sweden*
[2]*Department of Physics, FI-40014 University of Jyväskylä, Finland*

We report the first experimental determination of independent isomeric yield ratios using direct ion counting with a Penning trap, which offered such a high resolution in mass that isomeric states could be separated. The measurements were performed at the Ion Guide Isotope Separator On-Line (IGISOL) facility at the University of Jyväskylä. The isomer production ratios of ^{81}Ge, ^{96,97}Y, ^{128,130}Sn, and ^{129}Sb in the 25-MeV proton-induced fission of ^{nat}U and ^{232}Th were studied. Three isomeric pairs (^{81}Ge, ^{96}Y, and ^{129}Sb) were measured for the first time for the ^{nat}U(p, f) reaction, while all the reported yield ratios for the ^{232}Th(p, f) reaction were determined for the first time. The comparison of the experimentally determined isomeric yield ratios with data available in the literature shows a reasonable agreement, except for the case of ^{130}Sn for unspecified reasons. The obtained results were also compared with the GEF model, where good agreement can be noticed in most cases for both reactions. Serious discrepancies can only be observed for the cases of ^{96,97}Y for both reactions. Moreover, based on the isomeric yield ratios, the root-mean-square angular momenta (J_{rms}) of the fission fragments after scission were estimated using the TALYS code. The experimentally determined isomeric yield ratios, and consequently the deduced J_{rms}, for ^{130}Sn are significantly lower compared to ^{128}Sn for both fissioning systems. This can be attributed to the more spherical shape of the fragments that contribute to the formation of ^{130}Sn, due to their proximity to the $N = 82$ shell closure. The values of J_{rms} for ^{129}Sb are higher than ^{128}Sn for both reactions, despite the same neutron number of both nuclides ($N = 78$), indicating the odd-Z effect where fission fragments with odd-Z number tend to bear larger angular momentum than even-Z fragments. The isomer production ratio for the isotopes of Sn is more enhanced in the ^{nat}U(p, f) reaction than in ^{232}Th(p, f). The opposite is observed for ^{96}Y and ^{97}Y. These discrepancies might be associated to different scission shapes of the fragments for the two fission reactions, indicating the impact that the different fission modes can have on the isomeric yield ratios.

I. INTRODUCTION

One of the many open questions regarding the fission process is related to the origin of the angular momentum of the fission fragments [1]. It is thus desirable to obtain information on the angular momentum of the fragments as this can provide insight into the properties of the dynamical evolution of the fissioning nucleus from the saddle point until its descent to scission [2]. For a given fission mode, the final distribution of mass, charge, excitation energy, deformation, and angular momentum of the highly deformed nuclei are determined during this process.

Fission fragments produced in spontaneous or near-barrier fission have average angular momenta of about 6–8$\hbar$ [3–6]. As pointed out in a recent review by Andreyev *et al.* [1], although it is well established that the fission fragments carry

a considerable amount of angular momentum [7], it is still not fully comprehended how this is generated. Competing theories on this issue exist, which among others hypothesize thermal excitation [8–11] and/or quantum-mechanical uncertainty of angular-momentum-bearing modes [12] and Coulomb excitation after scission [13]. A strong coupling between the elongation and other collective degrees of freedom has also been considered [14]. At higher excitation energies, there are additional contributions to the fragment spins. Extra unpaired nucleons exist even at the saddle point, where the nucleus is highly excited. Moreover, excitations corresponding to collective modes in which the two nascent fragments move relative to one another have, as a result, a part of the initial angular momentum to be retained by the fragments [15].

The highly excited fission fragments de-excite by emission of neutrons and γ rays. The role of the average angular momentum of the primary fission fragments in this process is very important, as it controls the number of emitted neutrons and photons. However, so far the distribution of the angular momenta of the initial fragments cannot be measured directly, but it can be inferred from other fission observables like the isomeric yield ratios [16].

---

*vasileios.rakopoulos@physics.uu.se

†Corresponding author: mattias.lantz@physics.uu.se

‡Present address: Cyclotron Institute, Texas A&M University, 3366 TAMU, College Station, Texas 77843-3366, USA.

§Present address: SVAFO, Nyköping, Box 90, 61123, Sweden.

Isomers are nuclear states relatively long-lived compared to normal states in a particular nucleus or nuclear regime; in other words, they are metastable. The long lifetimes result from a combination of nuclear structure effects, such as spin and shape, inhibiting their decay. The main point is not whether the lifetimes are arbitrarily long or short, but rather that these unusually long lifetimes imply state of a different structure and an intrinsic state [17–21]. The obtained knowledge can be used for nuclear structure and astrophysics studies, especially since the r-process is believed to be terminated by the fission of very neutron-rich heavy nuclei [22]. In addition, the experimentally determined yields of metastable states in fission are necessary for calculations of the effect of delayed neutrons in nuclear reactors, since the β-delayed neutron emission probability from the metastable state can be notably different from that of the ground state, as, for example, in the case of ^{98}Y [23].

Furthermore, from the experimental determination of the isomeric yield ratios [24–31], the angular momentum of the initial fission fragments can be deduced using statistical model analysis [6,32]. This method can be used for all fission products, both with odd and even Z, but typically requires nuclides with suitable half-lives. The angular momentum can also be determined by other methods, such as (i) by measuring the angular distribution of prompt γ rays from the fission fragments [13,33–36], (ii) from the energy and multiplicity of prompt γ rays [4,37–39], and (iii) from the intensities of the cascade transitions to the ground state of the rotational bands [2]. All these methods have certain limitations, as, for example, (i) and (ii) can provide an estimate of the mass-averaged angular momentum and (iii) can only be used for even-even nuclides. Method (i) has been employed only in spontaneous fission of ^{252}Cf and thermal neutron-induced fission of actinides, while method (ii) has been used in both low- and medium-energy fission and can provide an estimate of the angular momentum for either one or both fragments for a given mass split, depending on how the γ-ray multiplicities were measured. In both these methods, and especially for low-energy fission, sawtooth behavior of the angular momentum was reported.

The isomeric yield ratios have usually been determined by means of γ spectroscopy, either by applying radiochemical separation (selection of Z) or by physical means using an ordinary isotope separator (selection of A). The results have been used to investigate collective rotational degrees of freedom [15,40–44]. However, there are several challenges in these techniques, such as insufficient mass resolving power (MRP) in the separator, difficulties to study refractory elements, and inadequate knowledge of decay schemes. Short-lived nuclei remain a challenge for both techniques.

The Ion Guide Isotope Separator On-Line (IGISOL) technique based on mass separation [45–47] is well suited for such experiments, as it is a fast and chemically insensitive method, facilitating measurements of short-lived fission products of any element. In case the isomeric yield ratios are measured by means of γ spectroscopy, as reported in Refs. [48–50], the fission fragments can be transported and detected within milliseconds. For ion counting with JYFLTRAP, as in the present study, the ions are detected within a few hundreds of ms from their creation.

A Penning trap can serve as a high-resolution mass separator, significantly improving the mass resolving power, as a resolution of $M/\Delta M \approx 10^5$ can be readily achieved. At the IGISOL facility [51] at the University of Jyväskylä, coupled to the superior mass resolving power of the JYFLTRAP [52], metastable states separated by a few hundred keV from the ground state can be resolved by using just the first (purification trap) of the two traps and employing the sideband cooling technique [53]. Thus, a direct ion counting measurement of the relative intensities between the states can be accomplished, even for fission products with half-lives as short as half a second. The IGISOL-JYFLTRAP technique has been used for measurements of independent isotopic yields [54,55], but this is the first time that it has been employed for the determination of isomeric yield ratios.

In this paper, we have produced fission fragments using the IGISOL method and applied novel ion trapping and counting techniques at the JYFLTRAP Penning trap to study isomeric yield ratios of ^{81}Ge, ^{96,97}Y, ^{128,130}Sn, and ^{129}Sb produced in the 25-MeV proton-induced fission of ^{nat}U and ^{232}Th. We present briefly the experimental technique in Sec. II and in Sec. III we describe the data analysis. In Secs. IV and V, the isomeric yield ratios from this work are presented, discussed, and compared with data available in the literature and with calculations performed with the GEF code [56,57]. In Sec. VI, the derivation of the root-mean-square angular momentum (J_{rms}) of the primary fission fragments using the reaction code TALYS [58] is described.

II. EXPERIMENTAL TECHNIQUE

The first measurement related to the present study, concerned the 25-MeV proton-induced fission of ^{232}Th and was performed in 2010 at the IGISOL-3 facility [60]. After that, the facility closed down for a major upgrade, in order to be recommissioned as IGISOL-4 in a new experimental hall [51]. In the upgraded facility, the fission of ^{232}Th and ^{nat}U induced by protons of the same energy were studied in various experimental campaigns. In both facilities, the proton beam from the K130 cyclotron was delivered to the ion guide [47], where the actinide target is mounted. The thicknesses of the ^{232}Th and ^{nat}U targets were 14 and 15 mg/cm^2, respectively.

Thin targets are one of the key features of the IGISOL technique [61,62], as a significant fraction of the fission products have enough recoil energy to escape from the target. A flow of helium buffer gas through the ion guide is used to thermalize the fission products. The reaction products are highly ionized in the nuclear reaction and their charge state is subsequently reduced due to collisions with helium atoms. A significant fraction of the products are singly charged due to the high first ionization potential of the buffer gas. The ions are extracted from the gas cell with the help of differential pumping and a sextupole ion guide (SPIG) [63] and electrostatically accelerated to 30q keV (where q is the charge of the ions, usually $q = 1$). A dipole magnet (MRP $\sim$ 500) is used to separate the isobaric chain of interest based on the mass-to-charge ratio (m/q). The continuous mass-separated beam is directed to the linear quadrupole radio-frequency cooler and buncher (RFQ) [64,65], where the ions are cooled by collisions

TABLE I. Information for the nuclides presented in this work. The metastable state is the higher spin state except for ^{81}Ge. All data are retrieved from Ref. [59].

| Nuclide | Ground state | | Metastable state | | | |
	Spin	$T_{1/2}$ (s)	E_{exc} (keV)	Spin	$T_{1/2}$ (s)	Decay mode
^{81}Ge	$9/2^+$	8 (2)	679.1	$(1/2^+)$	8 (2)	$\beta^- = 100\%$
^{96}Y	0^-	5.34 (5)	1540	8^+	9.6 (2)	$\beta^- = 100\%$
^{97}Y	$1/2^-$	3.75 (3)	667.5	$9/2^+$	1.17 (3)	$\beta^- > 99.3\%$, IT $< 0.7\%$
^{128}Sn	0^+	3544.2 (8.4)	2091.5	(7^-)	6.5 (5)	IT $= 100\%$
^{129}Sb	$7/2^+$	15717.6 (93.6)	1851.3	$(19/2^-)$	1062 (6)	$\beta^- = 85\%$, IT $= 15\%$
^{130}Sn	0^+	223.2 (4.2)	1946.9	7^-	102 (6)	$\beta^- = 100\%$

with buffer gas atoms and are subsequently released to the JYFLTRAP double Penning trap mass spectrometer [52] in short bunches of 10- to 15-μs duration.

JYFLTRAP consists of two cylindrical Penning traps. A magnetic field of 7.0 T is applied to the symmetry axis so that radial confinement of the ions can be achieved. The confinement in the third, axial direction is electrostatic. The motion of the trapped charged particles exhibits three different eigenmotions: the axial motion with the frequency ν_z, which occurs along the magnetic field lines, and two motions perpendicular to the magnetic field, the radial motions. The two radial motions are the magnetron motion, with the nearly mass-independent frequency ν_-, and the reduced cyclotron motion at the mass-dependent frequency ν_+. The sum of these two frequencies is in the ideal case equal to the cyclotron frequency ν_c [66].

In this work, we have employed the first trap as a high-resolution mass separator. By using the buffer-gas cooling technique [53], ions can be selectively centered and extracted out from the trap using a quadrupolar excitation at

$$\nu_{RF} = \nu_c = \frac{1}{2\pi}\frac{q}{m}B, \qquad (1)$$

where q and m are the charge and mass of the ion and B is the magnetic field. In this way, a direct ion counting measurement of the relative intensities between the states can be accomplished, even for short-lived fission products. Details of the method can be found in Refs. [52,53,67]. After extraction, the ions are guided to the end of the beam line, where they are registered in a microchannel plate (MCP) detector.

III. DATA ANALYSIS

Information on spin states, excitation energies, and decay modes of the nuclides studied in the present work are given in Table I. The recorded experimental data contain information on the cyclotron frequency, the time of flight (TOF) of the ions from the Penning trap to the detector, and the multiplicity on the MCP. The obtained spectra are cyclotron frequency spectra, inversely proportional to mass [see Eq. (1)].

A. Selection of the ions

All ions leave the purification trap with approximately the same energy, so primarily their TOF depends on their mass and charge. By performing a TOF gating, a selection of the desired

events can be achieved and background is almost completely suppressed.

In Fig. 1 a typical TOF spectrum is shown for mass $A = 97$. The ions with the desired mass form the most prominent peak in the spectrum. By applying a selection in the TOF range around this peak, the ions of interest are chosen to be further analyzed. The TOF range for this specific case is between 200 and 250 μs. Lighter ions, such as buffer gas impurities, have shorter TOF and appear in the lower part of the spectrum ($\sim$80 μs), while 2^+ and 3^+ charged β-decay daughters form peaks around 160 and 130 μs, respectively.

B. Determination of the peak intensities

The maximum transmission efficiency through the trap is achieved at the cyclotron frequency. Moreover, since the ionization mechanism is the fission itself and the shape and width of the peaks are invariant for given settings of the Penning trap, the height of the peak in the cyclotron frequency spectrum can be considered as a direct measurement of the yield of the nuclides. For the identification of the peaks appearing in the spectrum, a cyclotron frequency calibration based on the evaluated atomic masses [68] was performed at the beginning of each experiment by using xenon gas.

The isomeric yield ratios are determined in the form of the fraction of the high-spin state yield to the total yield of both
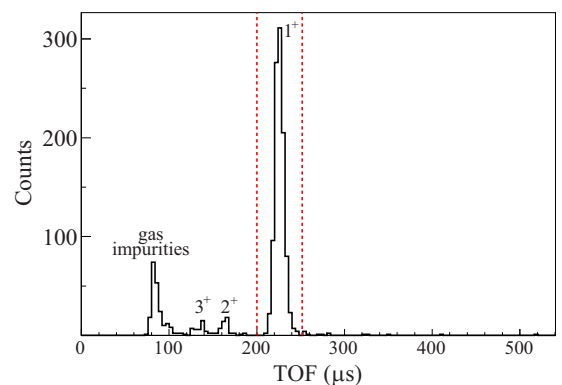

FIG. 1. A typical TOF spectrum, where the most prominent peak corresponds to the TOF of the ions with the desired mass ($A = 97$) after their purification. The red dashed lines represent the applied TOF gate (200–250 μs) for the selection of the ions. Ions that do not match the correct TOF are discarded from the analysis.
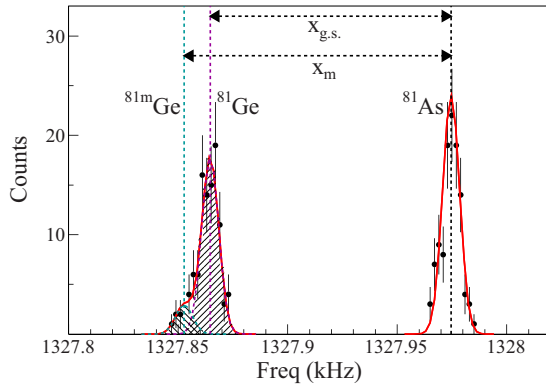
FIG. 2. Quadrupole frequency scan at $A = 81$. The peak positions (vertical dashed lines) of ^{81m}Ge and ^{81}Ge are calculated relative to ^{81}As, which is taken as reference. The peak identification is based on a frequency to mass calibration. The red line shows the fitted Gaussian functions used to extract the isomeric yield ratio. The shadowed areas under the peaks correspond to the number of detected nuclei for each state.

states:

$$R = \frac{Y_h}{Y_h + Y_l}. \quad (2)$$

For the purposes of this work, the intensities were determined by fitting a function, which consists of as many Gaussian functions as the number of states that are expected from the nuclear data tables in the measured frequency range. Since it can be assumed that the shape and the width of the peaks remain constant for the same trap measurement, as explained in the beginning of this section, the width for all Gaussian distributions in one spectrum is kept the same [see Eq. (3) below]. Metastable states that are lying close to the ground state might form multiplets, which are difficult to resolve. Thus, the positions of the two peaks of interest are taken relative to a reference peak, which is well defined and isolated in the spectrum. The relative positions are defined from their respective mass difference [68].

An example of a frequency spectrum can be seen in Fig. 2, where a frequency distribution spectrum for mass $A = 81$ is shown. Although three states of two different nuclides are expected in the spectrum, only two peaks can readily be resolved. This is because the metastable and the ground state of ^{81}Ge, only separated by 679 keV, are heavily overlapping. Thus, the positions of the ground and metastable states are taken relative to ^{81}As, which serves as the reference peak.

The fitted function for this particular example is presented in Eq. (3). This can be expanded to include all relevant states in the frequency range:

$$f(x) = A_1 e^{-\frac{(x - x_{\text{ref}})^2}{2\sigma^2}}$$
$$+ I \left[R\, e^{-\frac{(x - x_m)^2}{2\sigma^2}} + (1 - R) e^{-\frac{(x - x_{gs})^2}{2\sigma^2}} \right]. \quad (3)$$

In this equation, A_1 is the amplitude and x_{ref} is the position of the reference peak, x_m is the position of the metastable state, and x_{gs} is the position of the ground state, both taken

relative to the reference peak, I is the sum of the amplitudes of the multiplet peak ($I_m + I_{gs}$), R the deduced yield ratio as defined by Eq. (2), and σ is the width of the Gaussian function, restricted to be the same for all the peaks of the spectrum.

Of the aforementioned parameters, the position of the reference peak (x_{ref}) is a free parameter. Its starting guess value is taken from the mass to frequency calibration. The position of the metastable state and the ground state is defined by the relationship $x_y\; m_y = x_{\text{ref}}\; m_{\text{ref}}$, where y can be equal to m or gs. All the other parameters are fitted freely.

The stability of the system was studied for potential drift of frequency over the measuring time. Whenever unusual drifts were noticed, the analysis was performed for each scan. A scan is defined as a series of measurements of a number of ions detected in the MCP detector over a frequency range in steps of typically 1–2 Hz, which can be repeated several times. The result of R was then estimated as the weighted mean of these scans.

C. Corrections due to radioactive decay losses

In the present experiments, the time of one cycle, from the creation of the ions until their detection, varied from 404 to 1420 ms. During this time, radioactive β decays of short-lived isotopes may occur, so the registered intensities have to be corrected for such losses. Most of the time is spent on the collection of the ions in the RFQ cooler and buncher and the separation in the Penning trap. The ions are assumed to be accumulated in the cooler at a constant production rate, which is very close to the production rate at the ion guide since their transport from the ion guide to the cooler is performed within a few tens of μs. After a bunch of ions is extracted to the Penning trap, ions that decay in the trap are lost. Thus, the number of detected ions has to be corrected for these losses [69]. Decay corrections are important for isotopes with half-lives shorter than five times the length of the cycle [54]. In the current work, this criterion is fulfilled only for certain measurements of ^{96,97}Y and the applied corrections are in the range of 2–10%.

Contributions from precursors after their β decay do not need to be taken into account whether this may happen in the RFQ cooler and buncher or in the Penning trap. If the decay occurs in the cooler, the decay daughters are at least doubly charged, and since the confinement of the ions in the cooler is optimized for singly charged ions, it is unlikely for the products to remain in the cooler. β-decay products captured in the trap will be at least doubly charged and eventually be removed in the purification cycle, since the trap is tuned for singly charged ions. In the case that highly charged ions pass through the purification process [70] and reach the detector, their TOF will be significantly shorter and they are hence eliminated by the TOF gate (see Fig. 1).

D. Space charge and pile-up effects

As described in detail in Ref. [54], the size of the ion bunch plays a significant role on potential losses during the experiment. Specifically, the RFQ cooler and buncher and the purification trap can handle a certain number of ions. If this number is exceeded, then space charge effects may take

TABLE II. Isomeric yield ratios of 25-MeV proton-induced fission on ^{nat}U and ^{232}Th. In addition, the deduced values for the J_{rms} are reported. The indexes ι and $\jmath$ correspond to the number of emitted neutrons from the primary fragments. For all studied nuclides, except for ^{81}Ge, the emission of one or two neutrons are considered. For ^{81}Ge, the respective values are zero and one. For more information, see Sec. VI.

Nuclide	^{nat}U				^{232}Th			
	R	$J_{rms}^{n_\iota}(\hbar)$	$J_{rms}^{n_\jmath}(\hbar)$	$J_{rms}^{av}(\hbar)$	R	$J_{rms}^{n_\iota}(\hbar)$	$J_{rms}^{n_\jmath}(\hbar)$	$J_{rms}^{av}(\hbar)$
^{81}Ge	0.97 (1)	8.1 (1.5)		n.a.	0.92 (2)	5.3 (1.2)		n.a.
^{96}Y	0.55 (1)	6.9 (1)	10.7 (3)	8.9 (2)	0.61 (2)	7.4 (2)	18.7 (4)	12.7 (4)
^{97}Y	0.73 (2)	4.8 (4)	5.4 (3)	5.1 (4)	0.78 (2)	6.1 (4)	7.2 (5)	6.6 (4)
^{128}Sn	0.58 (2)	6.1 (2)	10.1 (5)	7.9 (4)	0.46 (1)	5.0 (1)	6.4 (1)	5.5 (1)
^{129}Sb	0.47 (4)	8.2 (4)	9.8 (7)	9.1 (6)	0.46 (1)	8.3 (1)	9.0 (1)	8.6 (1)
^{130}Sn	0.54 (2)	5.6 (2)	8.6 (3)	6.4 (2)	0.38 (1)	3.9 (1)	5.6 (1)	4.2 (1)

place. The cooler is reportedly able to handle 10^4 ions/bunches without significant losses [65] and the purification trap can tolerate a similar amount of ions/bunch without facing significant instability. However, the MCP detector cannot tolerate such large bunches of ions. It is capable of handling up to 10^7 ions/s, but if the ion bunch becomes too large, the time-resolving capability of the MCP might be exceeded. In this case, pile-up effects start to be observed as the implanted ions cannot be distinguished as separate signals, resulting in saturation of the number of detected ions. Saturation, in principle, can also occur because of space charge of some intense formed molecular beam. Detailed investigations have been performed at IGISOL in order to study the pile-up effect [54]. It has been concluded that it starts to affect significantly the results only when the ion bunch size increases above approximately 100 ions. During the current experiments, the pile-up was taken into consideration by keeping the bunch size at about 50 detected ions.

E. Sources of uncertainties

Relevant sources of uncertainties in this work emanate from the intensity of the mass peaks and the corrections due to radioactive decay losses. The former includes only the statistical ones that arise from the fit of the parameter R in Eq. (3). The parametrization of the fitted function was chosen so that the correlation of the two peaks of interest due to their overlap is taken into consideration. The latter depends on the uncertainties of the half-lives of decaying nuclei and on the timing parameters of the experiments. However, since these parameters are known accurately, their contribution to the uncertainty are expected to be insignificant.

Other systematic uncertainties that might affect the measurement concern the overall transport efficiency of IGISOL, which can be regarded as the product of the physical transport efficiency ϵ_p and the chemical transport efficiency ϵ_c [71]. The former depends on the operating conditions of the mass separator, while the latter depends on the chemical properties of the elements. However, since in the present study the production ratio of states of the same nuclides were studied, neither of the two uncertainties are relevant.

F. Impurities due to chemical effects

Chemical reactions of elements with gas impurities in the RFQ and the Penning trap can occur, since the ions spend

considerable time in these two apparatuses. Reactive elements, such as Zr, Y, etc., can form monoxide ions easily, resulting in contamination of the frequency spectra. Moreover, stable isotopes, such as ^{130}Xe, can disturb the measurements, as the space charge limit of the purification trap is reached, causing saturation in the detector, as mentioned earlier. Whenever such disturbances in the spectra were observed, these data were discarded from further analysis. More about the chemical effects and their significance and the influence of stable isotopes can be found in Ref. [54].

IV. RESULTS OF ISOMERIC YIELD RATIOS

In the present work, the isomeric yield ratios of six different isomeric pairs were determined experimentally and the results are shown in Table II. The given uncertainties include the statistical uncertainties and the uncertainties due to the radioactive decay loss corrections, as explained in Sec. III E.

The determined isomeric yield ratios cover a wide mass range, from $A = 81$ to $A = 130$. From the studied nuclides, ^{81}Ge is the only one which is located at the superasymmetric mass region, two of them are located at the asymmetric region of the light fragments (^{96,97}Y), while three are located at the edge of the symmetric mass region (^{128,130}Sn, ^{129}Sb). As has already been mentioned, the data were acquired in several experimental campaigns. Preliminary results for the isomer production ratios from each experimental campaign, after the data selection which is described in Sec. III F, can be found in Ref. [72].

In Fig. 3, the isomeric yield ratios as obtained in this work are shown for both fission reactions, together with results from calculations performed with the GEF code, version 2017/1.2, where only recently the proton-induced fission channel was introduced [56,57]. In addition, the results by Tanikawa et al. [48] are presented. In that work, the isomer ratios of the 24-MeV proton-induced fission of ^{238}U were measured at the Tohoku IGISOL facility in Japan, by means of γ spectroscopy. This is the only data set available in the literature that includes common nuclides with this work, for the same fissioning system and excitation energy.

V. DISCUSSION ON THE ISOMERIC YIELD RATIOS

The comparison of the results of the present study with the work by Tanikawa et al. [48] shows reasonable agreement for
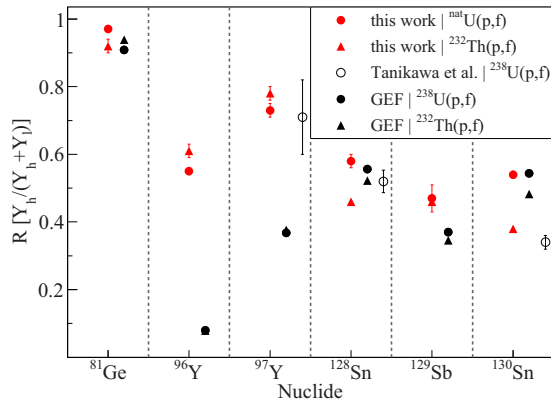
FIG. 3. Isomeric yield ratios for the six studied nuclei. Our results are shown in red circles (•) for the $^{nat}U(p, f)$ reaction and in red triangles (▲) for the $^{232}Th(p, f)$ reaction. In black markers, the results from the GEF code are depicted. The results by Tanikawa *et al.* [48] are also presented (○).
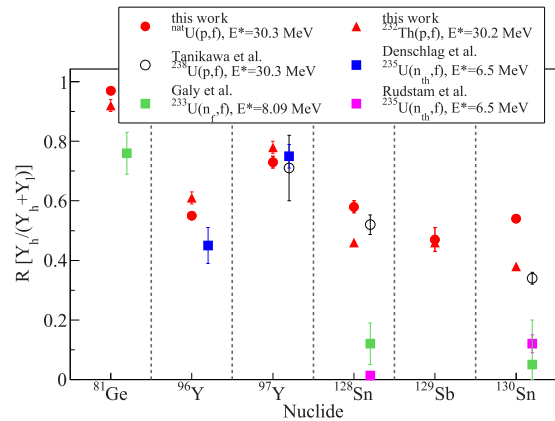

FIG. 4. The experimentally observed isomeric yield ratios from this work, compared with data available in the literature for different fissioning systems and excitation energies. The excitation energies (E^*) of each formed compound nucleus are given in the legend.

the yield ratios of ^{97}Y and ^{128}Sn. However, for the case of ^{130}Sn the result by Tanikawa *et al.* is significantly lower than ours.

The isomeric yield ratios from the GEF code are in good agreement with the experimental values for the cases of ^{128}Sn and ^{81}Ge for both fission reactions and ^{130}Sn for the $^{nat}U(p, f)$ reaction. On the other hand, for both reactions the code seems to underestimate significantly the isomeric yield ratios for the two Y isotopes. Slightly lower ratios were also predicted for ^{129}Sb. Despite the discrepancies in the results between the experimental values and the GEF calculations, it is worth mentioning that the isomeric yield ratios from the GEF code exhibit almost the same behavior as the experimental ones for the two reactions. Specifically, the yield ratios for the Sn isotopes are clearly higher for the fission of ^{nat}U compared to the fission of ^{232}Th, while for ^{96}Y and ^{97}Y the fission of ^{232}Th gives the same or higher results compared to the fission of ^{nat}U.

By comparing the experimental results for the two different fission reactions, it can be observed that the isomeric yield ratios of the $^{nat}U(p, f)$ reaction are significantly higher for the cases of ^{128,130}Sn and they are also larger for the case of ^{81}Ge. The opposite occurs for the two Y isotopes, ^{96,97}Y, where the isomeric yield ratios of the ^{232}Th(p, f) reaction are higher. The isomeric yield ratio of ^{129}Sb is the same for both reactions. Thus, we observe that for a given nuclide the high spin isomer production ratio exhibits dependency on the fissioning system. Since the excitation energies of the formed compound nuclei of the two studied systems are very close ($\sim$100 keV difference), the discrepancies of the results can hardly be attributed to the differences in excitation energies of the compound nuclei. As the isomeric yield ratios are related to the root-mean-square angular momentum (J_{rms}) of the primary fission fragments, and consequently to the deformation of the fragments at scission, as will be explained in more detail in Sec. VI A, the variations in the results might indicate different scission shapes of the fragments for the two fission reactions. According to the calculations performed with the GEF code, higher relative yield of the super long (SL) fission channel results in pronounced

population of the high-spin isomer, hinting that the fission modes may affect the isomeric yield ratio.

The importance of the excitation energy (E^*) of the compound nucleus on the isomeric yield ratios can be perceived in the following way: When a high amount of excitation energy is available, the initial spin of the fission fragments, and consequently the isomer production ratios, is expected to be higher due to the higher degree of freedom in collective motion [24,31]. Moreover, differences in the excitation energy will be reflected in differences in the de-excitation process. The de-excitation of higher excited fragments will result in the broadening of the fragment spin distribution in the E^*-J plane. Thus, especially when the primary fragment has higher spin than the high-spin isomer of the product, higher J will be trapped on the yrast line and consequently decay to the high-spin isomer.

The role that the excitation energy of the compound nucleus can play on the isomeric yield ratios can also be seen in Fig. 4, where the results of the present work are compared with close-lying fissioning systems at different excitation energies. These works concern proton-induced fission of ^{238}U [48], thermal neutron-induced fission of ^{235}U [73,74], and fast neutron-induced fission of ^{233}U [75]. They all have been performed in different facilities, but by means of γ spectroscopy. The study by Tanikawa *et al.* [48] has been realized at the Tohoku IGISOL facility at Japan. Both the work of Galy *et al.* [75] and Rudstam *et al.* [73] have been performed at the OSIRIS facility of the Studsvik Science Research Laboratory in Sweden, where the ISOL system was directly attached to a nuclear reactor. For the measurement by Denschlag *et al.* [74], the recoil mass separator LOHENGRIN at the Institut Laue-Langevin in Grenoble, France, has been employed.

From this comparison, one can see that the isomeric yield ratios for the various fissioning systems differ. The results of the current work are constantly higher, probably due to the particularly high excitation energy in the case of proton-induced fission. The differences of the angular momenta of the formed compound nuclei could also have an effect on the isomeric yield ratios but to a significant lesser degree,
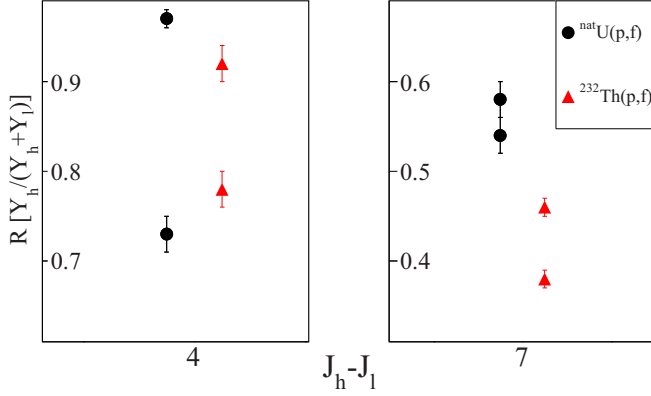
FIG. 5. The isomeric yield ratios of the nuclides with the same spin differences between the high-spin J_h and low-spin J_l states. On the left, the isomeric yield ratios of ^{81}Ge and ^{97}Y are shown ($\Delta J = 4$), and on the right, the results of ^{128,130}Sn ($\Delta J = 7$). Black circles (●) represent the ^{nat}U(p, f) reaction and red triangles (▲) represent the ^{232}Th(p, f) reaction.

since it is only partially retained by the fragments. Most of the induced angular momentum of the compound nucleus at higher excitation energies goes into orbital angular momentum of the fragments. This is highlighted in Ref. [31] for the α-induced fission of ^{238}U, in Ref. [15] where the isomer ratios of fission fragments at high excitation energies were studied, and in Ref. [43] where the dependence of fragment angular momentum on the entrance channel in ^{236}U fission was investigated. Surprisingly, the isomeric yield ratio of ^{97}Y seems rather insensitive to the fissioning system and excitation energy, as the result by Denschlag *et al.* [74] is very close to our fractional yield.

In Fig. 5 the isomeric yield ratio for different nuclei with the same spin difference between the high- and the low-spin state is depicted. On the left, the cases of ^{81}Ge and ^{97}Y are shown, where $\Delta J = 4$, and on the right the cases of ^{128,130}Sn, where $\Delta J = 7$. As can be seen from this figure, different results were obtained for nuclides with states of exactly the same spin difference. These discrepancies imply that the initial angular momentum of each primary fragment can also vary and that it is strongly case dependent.

VI. INITIAL ANGULAR MOMENTUM

A. Derivation of initial angular momentum

From the experimentally obtained isomeric yield ratios, it is not possible to deduce the spin distribution of the initial fission fragments. However, by assuming a functional form of the spin distribution of the primary fragments, their average angular momentum can be determined [24].

We used the TALYS code [58] in order to determine the dependency of the isomeric yield ratios on the root-mean-square angular momentum (J_{rms}) of the primary fragments. The calculations were performed for several J_{rms} values for a given excitation energy, until an agreement between the TALYS calculations and the experimental results was reached. Several different de-excitation paths of primary fragments can lead to the production of a specific fission product, depending on

the number of emitted neutrons. In the current investigation, for a specific isomeric pair, we take into account the mass dependence of post-scission neutron multiplicity [76], so that only the fragments that are most probable to contribute to this observable are considered.

Following Ref. [32], the fission fragments were assumed to be produced with a probability distribution $P(J)$ of the total angular momentum J,

$$P(J) \propto (2J + 1)\exp[-(J + 1/2)^2/2\sigma^2], \quad (4)$$

where we treat σ^2 as a free parameter, sometimes referred to as the spin cut-off parameter. The mean and the variance of this Rayleigh distribution are

$$\overline{J} = \sigma\sqrt{\pi/2} - 1/2, \quad \mathrm{Var}(J) = \frac{4 - \pi}{2}\sigma^2 \quad (5)$$

and the root mean square is given by

$$J_{\mathrm{rms}} = \sqrt{\overline{J}^2 + \mathrm{Var}(J)}. \quad (6)$$

The parameter σ can be related to the moment of inertia (I_0) and temperature (T) of the nucleus [77], as shown in Eq. (7). Consequently, and based on the assumption of statistical equilibrium among various collective modes [78], the root-mean-square angular momentum can also be related to the ground-state moment of inertia (I_0) and temperature (T) of the primary fragment:

$$\sigma^2 = \frac{I_0 T}{\hbar^2} \quad (7)$$

According to the pre-scission bending oscillation model [2,79], $\overline{J}$ can be related to the bending oscillation amplitude. The latter can be associated with the neck radius and semimajor axis at a certain deformation of the fission fragment [80]. Thus, assuming equal Coulomb and nuclear forces at the scission point [42], the fragment angular momentum can be related to the deformation via the semimajor axis.

1. Total excitation energy

We only consider binary fission, and the total excitation energy (TXE) of the fissioning system is, therefore, partitioned between the light (A_L, Z_L) and the heavy fragment (A_H, Z_H), as follows:

$$\begin{aligned}
\mathrm{TXE}&(A_L, Z_L, A_H, Z_H) \\
&= E_r^*(A_L, Z_L, A_H, Z_H) + S_p(A_C, Z_C) \\
&\quad + E_p - \mathrm{TKE}(A_L, A_H) - E_n, \quad (8)
\end{aligned}$$

where $S_p(A_C, Z_C)$ and E_p are the separation and the kinetic energies respectively of the compound nucleus for the proton-inducing fission. E_n is related to the multichance fission and takes into account the released energy of the pre-fission emitted particles. $E_r^*(A_L, Z_L, A_H, Z_H)$ is the energy release in the fission process given by the difference between the mass excesses of the compound nucleus and the fission fragments:

$$\begin{aligned}
E_r^*&(A_L, Z_L, A_H, Z_H) \\
&= M(A_C, Z_C) - M(A_L, Z_L) - M(A_H, Z_H). \quad (9)
\end{aligned}$$

The $\mathrm{TKE}(A_L, A_H)$ in Eq. (8) represents the distribution of the total kinetic energy of the fission fragments. Because of the absence of available information for the distribution of $\mathrm{TKE}(A_L, A_H)$ for the two reactions, we adopted the $\overline{\mathrm{TXE}(A_L, A_H)}$ from GEF, where multichance fission is taken into account.

How the total excitation energy is shared between the light and the heavy fission fragments is one of the long-standing questions about the nuclear fission process. In the present work, we use the assumption that the $\overline{\mathrm{TXE}}$ is partitioned according to the ratio of the average number of prompt neutrons emitted by complementary fragments [81]:

$$\overline{E}_H^* = \frac{\overline{\nu}_H}{\overline{\nu}_{\mathrm{pair}}}\overline{\mathrm{TXE}} \qquad \overline{E}_L^* = \left(1 - \frac{\overline{\nu}_H}{\overline{\nu}_{\mathrm{pair}}}\right)\overline{\mathrm{TXE}}, \qquad (10)$$

where $\overline{\nu}_{\mathrm{pair}} = \overline{\nu}_H + \overline{\nu}_L$ and $\overline{\nu}_H$ and $\overline{\nu}_L$ represent the average number of prompt neutrons emitted from the heavy and light fragments. The values of the post-scission neutron multiplicities of the fission fragments were taken from Refs. [76] and [82] for $^{\mathrm{nat}}$U and ^{232}Th, respectively.

2. Level density

In the de-excitation of a highly excited fission fragment, there is normally a distinction between two regions, the discrete part for the lower excitation energies and the continuum for the higher ones. The discrete level scheme in TALYS is based on the discrete level file of Belgya, as stored in the Reference Input Parameter Library (RIPL-3) database [58,83]. RIPL-3 contains the known level schemes and electromagnetic and γ-ray decay probabilities, which were compiled and available from the Evaluated Nuclear Structure Data File (ENSDF) in October 2007 [84]. For higher excitation energies, where discrete level information is not available or incomplete, nuclear level densities are used. The distinction of the two regions is rather arbitrary and it depends on the available information for the respective nucleus.

Out of the six implemented nuclear level density models in TALYS, we used two phenomenological models and one microscopical model in order to investigate the dependency of the results on the model. Specifically, the applied models were (i) the constant temperature Fermi gas model (CTFGM) [85], (ii) the back-shifted Fermi gas model (BSFGM) [86], and (iii) the microscopic level densities (MLD) as calculated by Goriely from drip line to drip line for excitation energies up to 150 MeV and for spin values up to $I = 30$, for the RIPL database [87].

In the CTFGM, which is the default in TALYS, the excitation energy range is divided into two main parts. For the low part, from 0 MeV excitation energy up to a matching energy E_M, the so-called constant temperature law applies. For the part above E_M, the Fermi gas model applies. In the BSFGM, the pairing energy is treated as an adjustable parameter and the Fermi gas expression is used to describe the level density at all energies. In the most contemporary versions of these phenomenological models, refinements such as energy-dependent shell effects and explicit treatment of collective effects are included.

B. Results and discussion

In Figs. 6 and 7, the isomeric yield ratio as a function of the parameter σ for the different level density models is shown for both fission reactions. The shadowed regions depict the experimental results with the respective uncertainties. For all studied nuclides, except for the case of ^{81}Ge, calculations for one or two neutrons emitted from the primary fragments were performed, as these emissions were considered most probable [76]. For ^{81}Ge, the emissions of zero and one neutrons were instead investigated.

As expected, the two phenomenological models seem to exhibit the same behavior for all nuclides. The only essential discrepancies between the two occur for both reactions in the cases of zero and one emitted neutrons in the production of ^{81}Ge and ^{130}Sn, respectively. In these cases, the results for the BSFG model are considerably lower for both reactions, and especially for ^{81}Ge, the calculations using the BSFG model could not reproduce the experimental result. When comparing with the MLD model, no safe conclusions can be drawn regarding general trends. As can be seen in Figs. 6 and 7, the MLD model sometimes gives lower values, as in the case of ^{97}Y, sometimes higher values, as in the cases of two emitted neutrons for the production of ^{128}Sn, ^{129}Sb, and ^{130}Sn, and it sometimes intersects with values of the CTFG and BSFG models. All the models show, as might be expected and with the exceptions mentioned above, a monotonic increase of the isomeric yield ratio R with respect to the σ (or J_{rms}) value.

For the case of ^{129}Sb, the code failed to reproduce the experimental value for both fission reactions even for very large values of σ when the level scheme from RIPL-3 was employed. An example of this is shown in Fig. 8 for the U(p, f) reaction and the MLD and BSFG models in the case of two emitted neutrons from the primary fragment. When the level scheme of ^{129}Sb was updated according to Ref. [88], the code was able to match the experimental isomeric yield ratio. Hence, the sensitivity of such calculations on the applied level scheme and the importance of adequate knowledge of those for the deduction of reliable results are highlighted.

For the case of ^{81}Ge, the code was unable to match the experimental isomeric yield ratio for $n = 1$, as the result was constantly equal to one ($R = 1$) independent of σ. This most likely occurs due to the low excitation energy of the primary fragment. For the $^{\mathrm{nat}}$U(p, f) reaction, the excitation energy of the fragment is just above the neutron separation energy (S_n) of ^{82}Ge, while for the ^{232}Th(p, f) reaction it is below. Thus, after the neutron emission, the remaining excitation energy of the secondary fragment is lower than the excitation energy of the $1/2^+$ state ($E_{\mathrm{exc}} = 697.1$ keV), making it impossible for this state to be populated after the γ-ray cascade. In reality, the excitation energy of the primary fragment follows a distribution with certain spread and not a single value; thus, there are contributions to the observed isomeric yield ratio from higher excited primary fragments. If no neutrons are assumed to be emitted from the primary fragment, the code was able to reproduce the experimental value for both reactions for the CTFG and MLD models, but not for the BSFGM.

In Table II, the results of the deduced angular momentum of the initial fragments are presented for the calculations made
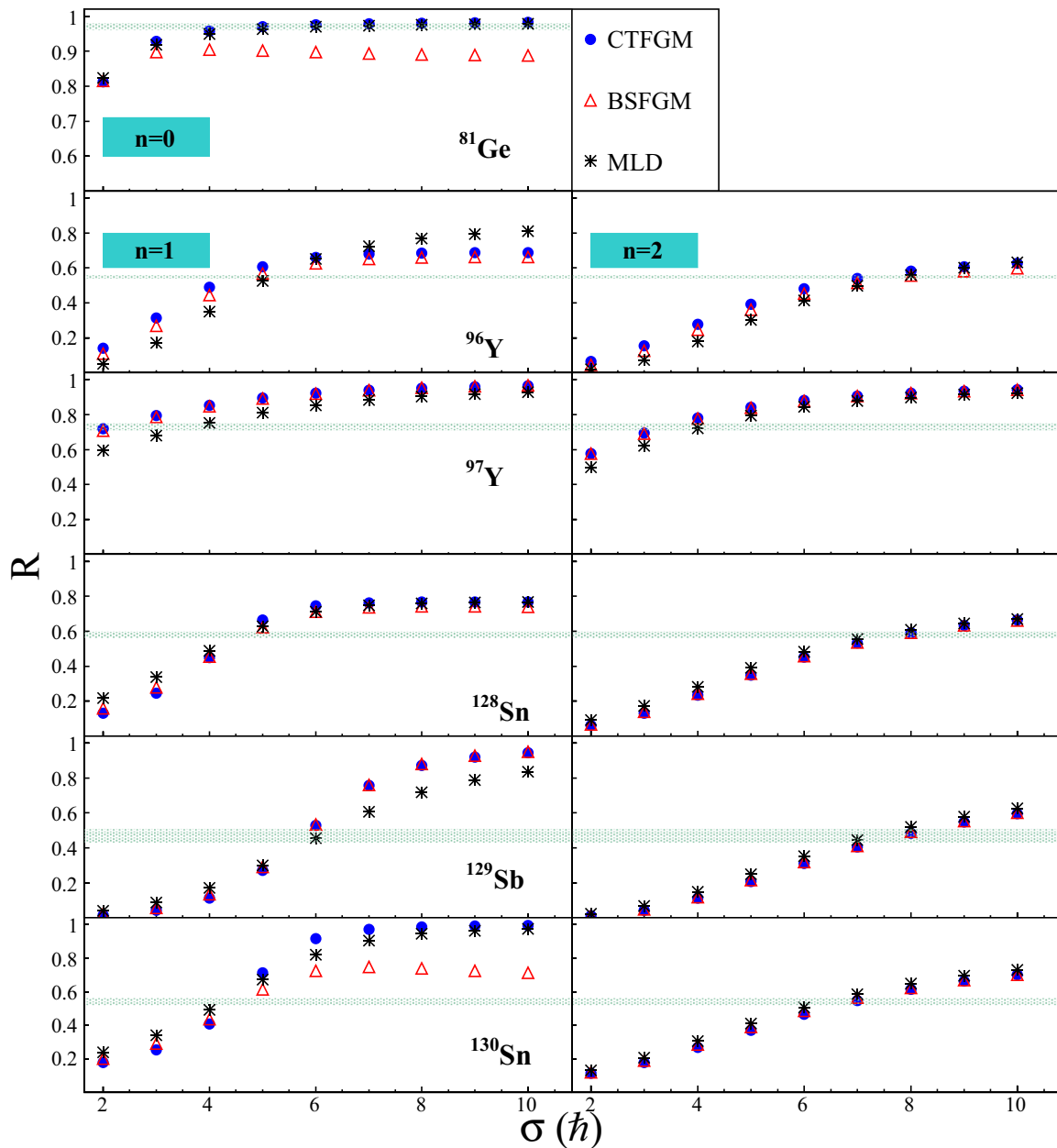
FIG. 6. The isomeric yield ratio as a function of σ of the primary fragment for different level density models as calculated in the present work for the $^{\mathrm{nat}}U(p, f)$ reaction. The shadowed green areas illustrate the experimental results with their respective uncertainties. For all nuclides, except for ^{81}Ge, the plots on the left show the isomeric yield ratio as the result of the de-excitation of the primary fragment after emitting one neutron ($n = 1$) and on the right after emitting two neutrons ($n = 2$). For ^{81}Ge, zero ($n = 0$) and one ($n = 1$) emitted neutrons were considered respectively. For more information, see Sec. VIB.

with the microscopic level density model. The values deduced with the other models show small differences and agree within uncertainties, except for the cases of ^{97}Y for one emitted neutron, where the results from the MLD model are slightly higher. $J_{\mathrm{rms}}^{n_\iota}$ and $J_{\mathrm{rms}}^{n_J}$ correspond to the results of different number of neutrons emitted from the primary fragments. The indexes ι and J are equal to one and two ($\iota = 1$, $J = 2$) for all nuclides, except for ^{81}Ge, where the respective values are $\iota = 0$ and $J = 1$, as mentioned earlier. J_{rms}^{av} corresponds to the mean of these results as weighted with the mass and charge distribution and the neutron emission probability of

the primary fragments. In the absence of experimental values for both fissioning systems, these values were taken from the GEF code [56,57]. Note that for ^{81}Ge, the code could not reproduce the experimental result for one emitted neutron emitted, and consequently the weighted mean could not be calculated. The estimated uncertainties of J_{rms} are derived from the experimental ones.

Since the data of the current study include only a small sample of the total produced fission products, it is difficult to conclude anything about the relation of the angular momentum and the fragment mass number. In Fig. 9, the results are
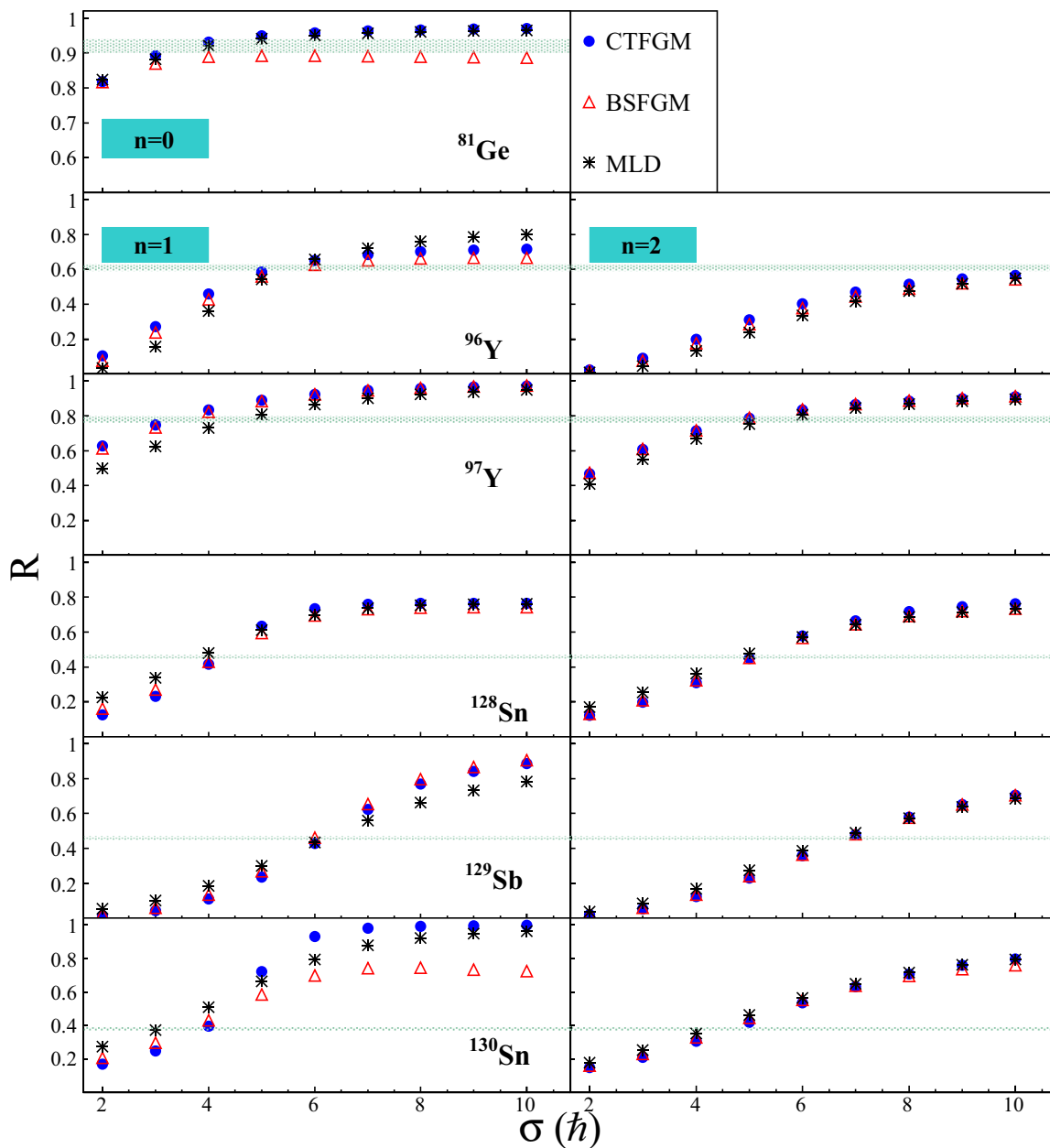
FIG. 7. Same as Fig. 6, but for the ^{232}Th(p, f) reaction. Note that for ^{96}Y, in the case of two emitted neutrons from the primary fragment, the crossing between the experimental value and the calculations performed with TALYS occurs outside the window range of the plot, at $\sigma = 13.6\hbar$.

plotted as a function of the neutron number of the fission product. As mentioned earlier, the conversion from σ to $J_{\rm rms}$ was performed by using Eq. (6). For both fissioning systems, some general remarks can be made regarding the deduced values of the angular momentum, since the tendency is similar. Specifically, it can be noticed that the $J_{\rm rms}$ values of ^{130}Sn are significantly lower than the corresponding values of ^{128}Sn for both fissioning systems. This can be attributed to the proximity of the fragments that contribute to ^{130}Sn to the $N = 82$ shell closure, thus having a more spherical shape and lower angular momentum.

The $J_{\rm rms}$ values of ^{129}Sb are considerably higher than ^{128}Sn for both reactions, despite the same neutron number of the two nuclides. Moreover, it is worth considering that the

experimentally determined isomeric yield ratio is noticeably lower for ^{129}Sb compared to ^{128}Sn for the $^{\rm nat}$U(p, f) reaction and the same for the ^{232}Th(p, f) reaction. The higher $J_{\rm rms}$ values of ^{129}Sb can be related to the odd-Z effect in the angular momentum of the fragment, as it has been observed that fragments with odd-Z are more deformed than the even-Z fragments, resulting in higher $J_{\rm rms}$ [42]. This effect may be caused by the polarization of the even-Z core by the extra unpaired proton, especially in the region of the $N = 82$ spherical shell, where the deformation energy surface might be more strongly governed by the protons, as explained in Ref. [89].

The large values of the angular momentum of ^{96}Y compared to ^{97}Y are remarkable, especially since the measured
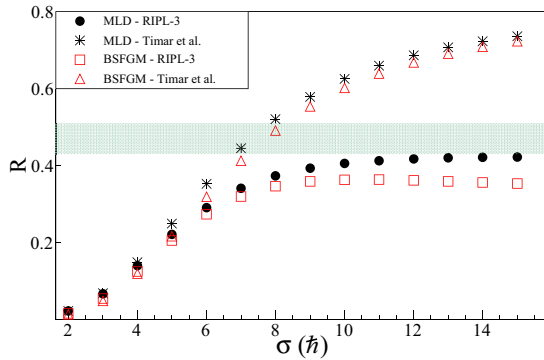
FIG. 8. The case of ^{129}Sb, where the calculations were performed with the level scheme of RIPL-3 and the updated level scheme from Ref. [88]. In red, the results for the BSFGM and in black for the MLD model.

isomeric yield ratios of the former are significantly lower. The intensively populated isomer of ^{97}Y has already been observed and reported in Refs. [48,90] and might be related to the sudden onset of deformation of nuclei with $Z \approx 40$ and $N \approx 60$ and the shape coexistence [90–92]. Although this could explain the higher isomeric yield ratio of ^{97}Y compared to ^{96}Y, the lower J_{rms} of ^{97}Y is still surprising. However, the J_{rms} value of ^{96}Y might be questionable, taking into account the limited knowledge of the level scheme of this nuclide [93].

From the comparison of the deduced angular momenta of the two fissioning systems, it can be noticed that higher values of J_{rms} are derived for the cases of ^{128,130}Sn and ^{129}Sb for the ^{nat}U(p, f) reaction, while ^{96,97}Y bear larger angular momenta in the case of the ^{232}Th(p, f) reaction. It is interesting that different trends on the J_{rms} are noticed depending on the fissioning system. As has already been mentioned in Sec. VI A, the J_{rms} of the fission fragments is related to the deformation of the fragments at the scission point. Thus, the higher isomeric yield ratios of ^{96,97}Y for the fission of ^{232}Th compared to the fission of ^{nat}U and hence the higher deduced J_{rms} values might be an indication of different shapes at scission.
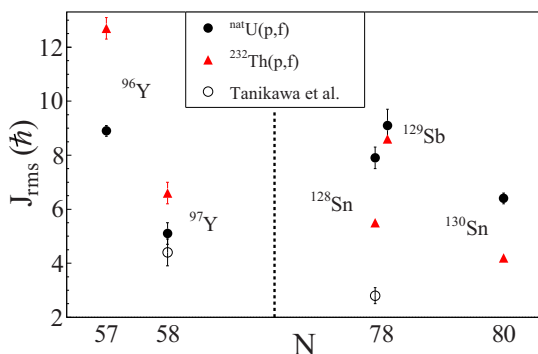

FIG. 9. The deduced J_{rms} for the two fissioning systems as a function of the neutron number of the fission products.

By comparing the J_{rms} values as derived from this work to the ones reported by Tanikawa *et al.* [48], where the deduction was performed using the statistical model method [6,32,94], a good agreement can be noticed for ^{97}Y. On the other hand, there is a significant difference for ^{128}Sn, even if the isomeric yield ratios are rather close to each other. There is no reported deduced value of J_{rms} for ^{130}Sn by Tanikawa *et al.*

VII. SUMMARY

In the current work, the isomeric yield ratios of six different pairs were measured for the 25-MeV proton-induced fission of ^{nat}U and ^{232}Th at the IGISOL-JYFLTRAP facilities at the University of Jyväskylä. Three of the pairs for the ^{nat}U(p, f) reaction were measured for the first time (^{81}Ge, ^{96}Y, and ^{129}Sb), while no data are available in the literature for any of the pairs for the ^{232}Th(p, f) reaction. It was the first time that the IGISOL-JYFLTRAP technique was employed for the measurements of isomer production ratios so that the yields could be determined with a direct ion counting method. Moreover, the root-mean-square angular momentum (J_{rms}) of the primary fission fragments was extracted based on the experimentally determined isomeric yield ratios, using the code TALYS.

From the experimentally observed ratios, there are indications of dependency of the results on the fissioning system. Specifically, the isomeric yield ratios of ^{128}Sn and ^{130}Sn for the ^{nat}U(p, f) reaction are significantly higher compared to the ^{232}Th(p, f) reaction. Moreover, it is worth mentioning that the isomeric yield ratio and consequently the J_{rms} of ^{128}Sn are higher compared to ^{130}Sn for the same fissioning system. This might result from the fact that the neutron number of the fragments that contribute to the production of ^{130}Sn are closer to the shell closure $N = 82$.

The deduced J_{rms} values of ^{129}Sb are considerably higher than the values of ^{128}Sn, although the isomeric yield ratio of ^{128}Sn is higher compared to ^{129}Sb for the ^{nat}U(p, f) reaction and identical for the ^{232}Th(p, f) reaction. The higher J_{rms} values of ^{129}Sb can be associated to the odd-Z effect, as fragments with odd proton number are more deformed and consequently bear higher angular momentum. Moreover, the importance of the requirement for sufficient knowledge of the level schemes for model calculations can also be noticed, as the experimental isomer production ratios could be reproduced by TALYS only after the level scheme was updated and implemented in the code.

The isomeric yield ratios are higher for ^{96}Y and ^{97}Y for the fission of ^{232}Th compared to the fission of ^{nat}U. According to the calculations performed with the GEF code, higher isomeric yield ratios have been noticed for higher relative yield of the super long (SL) fission channel for both fission reactions, hinting that the contribution of different fission modes may affect the angular momentum and hence the isomer production ratio as well. However, ^{129}Sb exhibits very similar isomeric yield ratios regardless of the reaction.

In order to decipher the discrepancies in the results between the two fission reactions and be able to draw safe conclusions regarding the dependency of the isomeric yield ratios on the fissioning system, access to new experimental results

with improved mass resolving power is considered essential. Because of the developments of the facility during 2017 [95], measurements of isomeric yield ratios can be determined by making use of the phase-imaging ion-cyclotron-resonance (PI-ICR) technique [96]. With this novel technique, the achievable MRP is significantly improved since both traps are used. Thus, it is possible to separate metastable states with excitation energies of a few tens of keV, such as the case of ^{129}Sn where the high-spin isomer is separated from the ground state by 35 keV. This will be reported in forthcoming publications together with results obtained with this technique for the odd-mass Cd and In isotopes in the mass range $A = 119$–127.

[1] A. N. Andreyev, K. Nishio, and K.-H. Schmidt, Rep. Prog. Phys. **81**, 016301 (2018).

[2] J. B. Wilhelmy, E. Cheifetz, R. C. Jared, S. G. Thompson, H. R. Bowman, and J. O. Rasmussen, Phys. Rev. C **5**, 2041 (1972).

[3] T. D. Thomas and J. R. Grover, Phys. Rev. **159**, 980 (1967).

[4] F. Pleasonton, R. L. Ferguson, and H. W. Schmitt, Phys. Rev. C **6**, 1023 (1972).

[5] P. Armbruster, H. Labus, and K. Reichelt, Z. Naturforsch. **26a**, 512 (1971).

[6] J. R. Huizenga and R. Vandenbosch, Phys. Rev. **120**, 1305 (1960).

[7] R. Vandenbosch and J. R. Huizenga, *Nuclear Fission* (Academic Press, New York, 1973).

[8] L. G. Moretto and G. J. Wozniak, Pramana J. Phys. **33**, 209 (1989).

[9] Ş. Mişicu, A. Săndulescu, G. M. Ter-Akopian, and W. Greiner, Phys. Rev. C **60**, 034613 (1999).

[10] T. M. Shneidman, G. G. Adamian, N. V. Antonenko, S. P. Ivanova, R. V. Jolos, and W. Scheid, Phys. Atom. Nucl. **66**, 206 (2003).

[11] F. Gönnenwein, I. Tsekhanovich, and V. Rubchenya, Int. J. Mod. Phys. E **16**, 410 (2007).

[12] L. Bonneau, P. Quentin, and I. N. Mikhailov, Phys. Rev. C **75**, 064313 (2007).

[13] M. M. Hoffman, Phys. Rev. **133**, B714 (1964).

[14] A. Bulgac, P. Magierski, K. J. Roche, and I. Stetcu, Phys. Rev. Lett. **116**, 122504 (2016).

[15] J. G. Cuninghame, J. A. B. Goodall, J. E. Freeman, G. W. A. Newton, V. J. Robinson, J. L. Durrell, G. S. Foote, I. S. Grant, and M. Rathle, J. Phys. G **6**, 127 (1980).

[16] I. Stetcu, P. Talou, T. Kawano, and M. Jandel, Phys. Rev. C **88**, 044603 (2013).

[17] P. Walker and G. Dracoulis, Nature (London) **399**, 35 (1999).

[18] G. D. Dracoulis, P. M. Walker, and F. G. Kondev, Rep. Prog. Phys. **79**, 076301 (2016).

[19] F. G. Kondev, G. D. Dracoulis, and T. Kibédi, At. Data Nucl. Data Tables **103–104**, 50 (2015).

[20] A. Aprahamian and Y. Sun, Nat. Phys. **1**, 81 (2005).

[21] A. K. Jain, B. Maheshwari, S. Garg, M. Patial, and B. Singh, Nucl. Data Sheets **128**, 1 (2015).

[22] M. Arnould, S. Goriely, and K. Takahashi, Phys. Rep. **450**, 97 (2007).

[23] T. R. England, W. B. Wilson, R. E. Schenter, and F. M. Mann, Nucl. Sci. Eng. **85**, 139 (1983).

[24] D. G. Sarantites, G. E. Gordon, and C. D. Coryell, Phys. Rev. **138**, B353 (1965).

[25] H. O. Denschlag, H. Braun, W. Faubel, G. Fischbach, H. Meixler, G. Paffarth, W. Porsch, M. Weis, H. Schrader, G. Siegert *et al.*, in *Proceedings of the Fourth IAEA Symposium on Physics and Chemistry of Fission, Julich, 1979* (IAEA, Vienna, 1980), Vol. 2, p. 153.

[26] J. P. Bocquet, F. Schussler, E. Monnand, and K. Sistemich, in *Proceedings of the Fourth IAEA Symposium on Physics and Chemistry of Fission, Julich, 1979* (IAEA, Vienna, 1980), Vol. 2, p. 179.

[27] D. C. Aumann and W. Gückel, Phys. Rev. C **16**, 160 (1977).

[28] G. P. Ford, K. Wolfsberg, and B. R. Erdal, Phys. Rev. C **30**, 195 (1984).

[29] I. Fujiwara, N. Imanishi, and T. Nishi, J. Phys. Soc. Jpn. **51**, 1713 (1982).

[30] N. Imanishi, I. Fujiwara, and T. Nishi, Nucl. Phys. A **263**, 141 (1976).

[31] B. S. Tomar, A. Goswami, S. K. Das, B. K. Srivastava, R. Guin, S. M. Sahakundu, and S. Prakash, Phys. Rev. C **38**, 1787 (1988).

[32] R. Vandenbosch and J. R. Huizenga, Phys. Rev. **120**, 1313 (1960).

[33] V. M. Strutinsky, Sov. Phys. JETP **10**, 613 (1960).

[34] J. H. Hamilton, A. V. Ramayya, J. K. Hwang, J. Kormicki, B. R. S. Babu, A. Sandulescu, A. Florescu, W. Greiner, G. M. Ter-Akopian, Y. T. Oganessian *et al.*, Prog. Part. Nucl. Phys. **38**, 273 (1997).

[35] W. Urban, J. L. Durell, W. R. Phillips, A. G. Smith, M. A. Jones, I. Ahmad, A. R. Barnett, M. Bentaleb, S. J. Dorning, M. J. Leddy *et al.*, Z. Phys. A **358**, 145 (1997).

[36] A. G. Smith, G. S. Simpson, J. Billowes, P. J. Dagnall, J. L. Durell, S. J. Freeman, M. Leddy, W. R. Phillips, A. A. Roach, J. F. Smith *et al.*, Phys. Rev. C **60**, 064611 (1999).

[37] S. A. Johansson, Nucl. Phys. **60**, 378 (1964).

[38] S. A. Johansson, Nucl. Phys. **64**, 147 (1965).

[39] H. Nifenecker, C. Signarbieux, M. Ribrag, J. Poitou, and J. Matuszek, Nucl. Phys. A **189**, 285 (1972).

[40] H. Naik, T. Datta, S. P. Dange, P. K. Pujari, S. Prakash, and M. V. Ramaniah, Z. Phys. A **331**, 335 (1988).

[41] H. Naik, S. P. Dange, and R. J. Singh, Phys. Rev. C **71**, 014304 (2005).

[42] T. Datta, S. P. Dange, S. K. Das, S. Prakash, and M. V. Ramaniah, Z. Phys. A **324**, 81 (1986).

[43] T. Datta, S. M. Sahakundu, S. P. Dange, N. Chakravarty, R. Guin, and S. Prakash, Phys. Rev. C **28**, 1206 (1983).

[44] A. Bail, O. Serot, L. Mathieu, O. Litaize, T. Materna, U. Köster, H. Faust, A. Letourneau, and S. Panebianco, Phys. Rev. C **84**, 034605 (2011).

[45] J. Ärje, J. Äystö, H. Hyvönen, P. Taskinen, V. Koponen, J. Honkanen, A. Hautojärvi, and K. Vierinen, Phys. Rev. Lett. **54**, 99 (1985).

[46] J. Äystö, Nucl. Phys. A **805**, 162c (2008).

[47] I. D. Moore, P. Dendooven, and J. Ärje, Hyperfine Interact. **223**, 17 (2014).

[48] M. Tanikawa, H. Kudo, H. Sunaoshi, M. Wada, T. Shinozuka, and M. Fujioka, Z. Phys. A **347**, 53 (1993).

[49] S. Goto, D. Kaji, H. Kudo, M. Fujita, T. Shinozuka, and M. Fujioka, J. Radioanal. Nucl. Chem. **239**, 109 (1999).

[50] A. Mattera, S. Pomp, M. Lantz, V. Rakopoulos, A. Solders, A. Al-Adili, H. Penttilä, I. D. Moore, S. Rinta-Antila, T. Eronen *et al.*, Eur. Phys. J. A **54**, 33 (2018).

[51] I. D. Moore, T. Eronen, D. Gorelov, J. Hakala, A. Jokinen, A. Kankainen, V. S. Kolhinen, J. Koponen, H. Penttilä, I. Pohjalainen *et al.*, Nucl. Instrum. Methods Phys. Res. B **317**, 208 (2013).

[52] T. Eronen, V. S. Kolhinen, V. V. Elomaa, D. Gorelov, U. Hager, J. Hakala, A. Jokinen, A. Kankainen, P. Karvonen, S. Kopecky *et al.*, Eur. Phys. J. A **48**, 46 (2012).

[53] G. Savard, St. Becker, G. Bollen, H.-J. Kluge, R. B. Moore, Th. Otto, L. Schweikhard, H. Stolzenberg, and U. Wiess, Phys. Lett. A **158**, 247 (1991).

[54] H. Penttilä, P. Karvonen, T. Eronen, V. V. Elomaa, U. Hager, J. Hakala, A. Jokinen, A. Kankainen, I. D. Moore, K. Peräjärvi *et al.*, Eur. Phys. J. A **44**, 147 (2010).

[55] H. Penttilä, D. Gorelov, V. V. Elomaa, T. Eronen, U. Hager, J. Hakala, A. Jokinen, A. Kankainen, P. Karvonen, I. D. Moore *et al.*, Eur. Phys. J. A **52**, 104 (2016).

[56] K.-H. Schmidt, B. Jurado, and C. Amouroux, General description of fission observables, JEFF Report 24 GEF Model, NEA-DB-DOC–2014-1, Nuclear Energy Agency of the OECD (NEA), 2014.

[57] K.-H. Schmidt, B. Jurado, C. Amouroux, and C. Schmitt, Nucl. Data Sheets **131**, 107 (2016).

[58] A. J. Koning, S. Hilaire, and M. C. Duijvestijn, in *International Conference on Nuclear Data for Science and Technology* (EDP Sciences, Nice, 2007).

[59] G. Audi, F. G. Kondev, M. Wang, W. J. Huang, and S. Naimi, Chin. Phys. C **41**, 030001 (2017).

[60] H. Penttilä *et al.*, in *The Fourth International Conference on Exotic Nuclei and Atomic Masses*, edited by C. J. Gross, W. Nazarewicz, and K. P. Rykaczewski (Springer, Berlin, 2005), pp. 745–747.

[61] J. Äystö, Nucl. Phys. A **693**, 477 (2001).

[62] A. Al-Adili, K. Jansson, M. Lantz, A. Solders, D. Gorelov, C. Gustavsson, A. Mattera, I. Moore, A. V. Prokofiev, V. Rakopoulos *et al.*, Eur. Phys. J. A **51**, 59 (2015).

[63] P. Karvonen, I. D. Moore, T. Sonoda, T. Kessler, H. Penttilä, K. Peräjärvi, P. Ronkanen, and J. Äystö, Nucl. Instrum. Methods Phys. Res. B **266**, 4794 (2008).

[64] A. Nieminen, J. Huikari, A. Jokinen, J. Äystö, P. Campbell, and E. C. A. Cochrane, Nucl. Instrum. Methods Phys. Res. A **469**, 244 (2001).

[65] A. Nieminen, P. Campbell, J. Billowes, D. H. Forest, J. A. R. Griffith, J. Huikari, A. Jokinen, I. D. Moore, R. Moore, G. Tungate, and J. Äystö, Phys. Rev. Lett. **88**, 094801 (2002).

[66] G. Gabrielse, Int. J. Mass Spectom. **279**, 107 (2009).

[67] V. S. Kolhinen, S. Kopecky, T. Eronen, U. Hager, J. Hakala, J. Huikari, A. Jokinen, A. Nieminen, S. Rinta-Antila, J. Szerypo, and J. Äystö, Nucl. Instrum. Methods Phys. Res. A **528**, 776 (2004).

[68] M. Wang, G. Audi, F. G. Kondev, W. J. Huang, S. Naimi, and X. Xu, Chin. Phys. C **41**, 030003 (2017).

[69] D. Gorelov, Ph.D. thesis, University of Jyväskylä, Finland, 2015.

[70] A. Herlert *et al.*, New J. Phys. **7**, 44 (2005).

[71] H. Kudo, M. Maruyama, M. Tanikawa, T. Shinozuka, and M. Fujioka, Phys. Rev. C **57**, 178 (1998).

[72] V. Rakopoulos, M. Lantz, A. Al-Adili, D. Gorelov, A. Jokinen, V. Kolhinen, A. Mattera, I. D. Moore, H. Penttilä, A. V. Prokofiev *et al.*, EPJ Web Conf. **146**, 04054 (2017).

[73] G. Rudstam, P. Aagaard, and H.-U. Zwicky, Yields of products from thermal-neutron induced fission of ^{235}U, NFL-42, Studsvik Science Research Laboratory, Nyköping, Sweden, 1985.

[74] H. O. Denschlag, W. Ditz, H. Faust, U. Güttler, and S. Hörner, Progress report on nuclear data research in the Federal Republic of Germany, International Atomic Energy Agency, Vienna, Austria, 1985.

[75] J. Galy, B. Fogelberg, F. Storrer, and H. Mach, Eur. Phys. J. A **8**, 331 (2000).

[76] V. A. Rubchenya, W. H. Trzaska, D. N. Vakhtin, J. Äystö, P. Dendooven, S. Hankonen, A. Jokinen, Z. Radivojevich, J. C. Wang, I. D. Alkhazov *et al.*, Nucl. Instrum. Methods Phys. Res. A **463**, 653 (2001).

[77] T. Ericson, Nucl. Phys. **11**, 481 (1959).

[78] J. R. Nix and W. J. Swiatecki, Nucl. Phys. **71**, 1 (1965).

[79] J. O. Rasmussen, W. Nörenberg, and H. J. Mang, Nucl. Phys. A **136**, 465 (1969).

[80] H. Schultheis and R. Schultheis, Phys. Rev. C **18**, 1317 (1978).

[81] C. Manailescu, A. Tudora, F.-J. Hambsch, C. Morariu, and S. Oberstedt, Nucl. Phys. A **867**, 12 (2011).

[82] S. Isaev, R. Prieels, Th. Keutgen, J. Van Mol, Y. El Masri, and P. Demetriou, Nucl. Phys. A **809**, 1 (2008).

[83] R. Capote, M. Herman, P. Obložinský, P. G. Young, S. Goriely, T. Belgya, A. V. Ignatyuk, A. J. Koning, S. Hilaire, V. A. Plujko *et al.*, Nucl. Data Sheets **110**, 3107 (2009).

[84] M. R. Bhat, in *Nuclear Data Science Technology*, edited by S. M. Qaim (Springer, Berlin, 1992), pp. 817–821.

[85] A. Gilbert and A. G. W. Cameron, Can. J. Phys. **43**, 1446 (1965).

[86] W. Dilg, W. Schantl, H. Vonach, and M. Uhl, Nucl. Phys. A **217**, 269 (1973).

[87] S. Goriely, F. Tondeur, and J. M. Pearson, At. Data Nucl. Data Tables **77**, 311 (2001).

[88] J. Timar, Z. Elekes, and B. Singh, Nucl. Data Sheets **121**, 143 (2014).

[89] V. A. Madsen and V. R. Brown, Phys. Rev. Lett. **52**, 176 (1984).

[90] B. Cheal, M. D. Gardner, M. Avgoulea, J. Billowes, M. L. Bissell, P. Campbell, T. Eronen, K. T. Flanagan, D. H. Forest, J. Huikari *et al.*, Phys. Lett. B **645**, 133 (2007).

[91] K. Heyde and J. L. Wood, Rev. Mod. Phys. **83**, 1467 (2011).

[92] U. Hager, A. Jokinen, V.-V. Elomaa, T. Eronen, J. Hakala, A. Kankainen, S. Rahaman, J. Rissanen, I. D. Moore, S. Rinta-Antila *et al.*, Nucl. Phys. A **793**, 20 (2007).

[93] Ł. W. Iskra, B. Fornal, S. Leoni, G. Bocchi, A. Petrovici, C. Porzio, A. Blanc, G. De France, M. Jentschel, U. Köster *et al.*, Europhys. Lett. **117**, 12001 (2017).

[94] H. Warhanek and R. Vandenbosch, J. Inorg. Nucl. Chem. **26**, 669 (1964).

[95] JYFL Accelerator News 25, 2 (2017), https://www.jyu.fi/science/en/physics/current/jyfl-accelerator-news/newsletter-2.pdf.

[96] S. Eliseev, K. Blaum, M. Block, C. Droese, M. Goncharov, E. Minaya Ramirez, D. A. Nesterenko, Yu. N. Novikov, and L. Schweikhard, Phys. Rev. Lett. **110**, 082501 (2013).